# JCTC
Journal of Chemical Theory and Computation

Investigation of a Quantum Monte Carlo Protocol To Achieve High Accuracy and High-Throughput Materials Formation Energies

Kayahan Saritas,[†] Tim Mueller,[‡] Lucas Wagner,[¶] and Jeffrey C. Grossman[*,†]

[†]Department of Materials Science and Engineering, Massachusetts Institute of Technology, Cambridge, Massachusetts 02139, United States

[‡]Department of Materials Science and Engineering, Johns Hopkins University, Baltimore, Maryland 21218, United States

[¶]Department of Physics, University of Illinois at Urbana−Champaign, Urbana−Champaign, Illinois 61801, United States

S *Supporting Information*

ABSTRACT: High-throughput calculations based on density functional theory (DFT) methods have been widely implemented in the scientific community. However, depending on both the properties of interest as well as particular chemical/structural phase space, accuracy even for correct trends remains a key challenge for DFT. In this work, we evaluate the use of quantum Monte Carlo (QMC) to calculate material formation energies in a high-throughput environment. We test the performance of automated QMC calculations on 21 compounds with high quality reference data from the Committee on Data for Science and Technology (CODATA) thermodynamic database. We compare our approach to different DFT methods as well as different pseudopotentials, showing that errors in QMC calculations can be progressively improved especially when correct pseudopotentials are used. We determine a set of accurate pseudopotentials in QMC via a systematic investigation of multiple available pseudopotential libraries. We show that using this simple automated recipe, QMC calculations can outperform DFT calculations over a wide set of materials. Out of 21 compounds tested, chemical accuracy has been obtained in formation energies of 11 structures using our QMC recipe, compared to none using DFT calculations.

$$\Psi(\{r_i\},\{r_j\})=exp[J(\{r_i\},\{r_j\}]D(\{r_j\})$$

ΔH_f @ 0 K
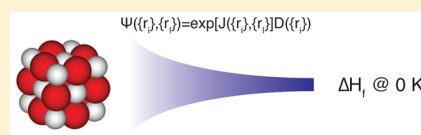
1. INTRODUCTION

The emergence of the field of materials informatics promises to accelerate the design and development of new materials through the creation and analysis of large databases of material properties. Such databases may be searched to identify promising materials or analyzed to identify important chemical and structural trends, providing new insights into how to create materials with desired properties. Material property databases may also serve as valuable sources of reference data; for example, databases of material energies may be used to estimate the thermodynamic stability of a new material by enabling the rapid comparison of its calculated energy to the precalculated energies of all known possible decomposition products.[1,2]

Rapid increases in the speed of computers have made it possible to populate material property databases using high-throughput calculations. However, the degree to which such databases are useful depends on the quality of the underlying data. One of the most popular methods for high-throughput calculations of material properties is density functional theory[3,4] (DFT) using the generalized gradient approximation (GGA).[5] Cancellation of errors makes DFT a useful tool for comparing materials and molecules in which the chemical environments of the atoms do not significantly change. However, in some cases, such as when the oxidation state or local chemical environment of an element changes, cancellation of errors can break down, and the error in DFT/GGA can be significant.[6−8] Although it may be possible to correct for these errors by referencing to empirical data, accurate reference data are not always available. For example, although there are more than 100,000 material

entries in the ICSD, there are fewer than 1,000 known material enthalpies of formation in the NIST-JANAF tables.[9]

To improve upon the accuracy of the computational data stored in materials databases, researchers have investigated a number of alternatives to DFT/GGA for high-throughput calculations, including hybrid DFT, DFT+U, and GW calculations.[10,11] The computational expense of these methods can be significantly greater than that of DFT/GGA, but this expense can often be justified if the calculated data is heavily reused. However, it is important that a method used for the high-throughput calculation of material properties is scalable (both with system size and with number of computing processors) and generally applicable to a wide variety of materials. With these goals in mind quantum Monte Carlo (QMC) is one of the most promising methods for high-throughput, accurate calculations of material properties.[12,13]

Quantum Monte Carlo refers to a family of statistical methods for approximating a solution to the many-body Schrödinger equation in a way that explicitly accounts for both the antisymmetry of the many-body wave function and electron correlation. In this paper we have used a form of quantum Monte Carlo known as diffusion Monte Carlo (DMC), described in section 2.1. Because it relies on statistical sampling, diffusion Monte Carlo scales nearly perfectly linearly with the number of available processing cores up to tens of thousands of processors, making it very well suited for modern high

A

performance computing architectures. For systems containing up to several hundred atoms the time required to reach a given error bar scales effectively as N^4,[14,15] and N^3 scaling is often realized in practice.[15] Even better scaling can be realized if local orbitals are used.[16,17] Because the error bars on the calculation are inversely proportional to the square root of the simulation time, the time required to achieve a given standard error per atom effectively scales linearly or better with system size.[18] This scalability with system size sets DMC apart from other highly accurate quantum chemical methods such as coupled cluster, which typically scale as N^5 to N^7.[19]

There is great promise in the potential use of DMC to populate databases of highly accurate material formation energies. Databases of material energies enable the construction of zero-temperature phase diagrams that provide a baseline for temperature-dependent phase diagrams.[1,2] Such phase diagrams allow researchers to estimate the thermodynamic stability and chemical reactivity of a new material before it has been synthesized, enabling experimental efforts to focus only on materials that are most likely to exist and be stable in operating conditions. In such applications the relevant quantity is the formation energy per atom. Because DMC effectively scales linearly with system size when calculating energies per atom, it can be practically used to calculate formation energies for materials with up to hundreds of atoms per unit cell. Unlike some highly accurate quantum chemical methods that do not work well for crystals or metals, DMC has been shown to provide accurate energies for a variety of molecules[20] and materials including metals, insulators, and semiconductors.[21]

The use of QMC in automated, high-throughput calculations is an emerging area of research. Shulenburger and Mattsson[12] investigated equilibrium lattice constants and bulk moduli of several solids. Krogel[22] also developed an automated code for QMC workflows that were used to calculate formation energies and lattice constants of several binary oxides.[23] Here we assess the use of QMC in high-throughput calculations of material formation energies, following previous work that demonstrated DMC is capable of accurately calculating cohesive energies,[21,24] electronic band gaps,[25] and accurate phase diagrams under extreme pressures.[26]

Despite the accuracy of DMC in material energies, the degree of automation that can be performed over the DMC calculations is sometimes unclear. We have used DMC to calculate the 0 K formation energies for 21 materials for which highly accurate experimental data exists. There are many choices to be made when using DMC to calculate the energy of a material, and it is typically preferable to carefully choose the settings and algorithms that are expected to work best for a given system. However, such an approach is not practical for high-throughput calculations of tens of thousands of materials. To assess the practicality of using DMC on such a large scale, we have performed our tests in an automated way that required minimal manual adjustments. In the following sections we present the methodology of our approach, the results of our calculations, and an analysis of the areas that we believe will require the most additional work.

2. METHODS

2.1. Diffusion Monte Carlo. Here we provide a brief overview of the diffusion Monte Carlo approach. Additional details can be found in refs 15, 18, and 27. Diffusion Monte Carlo solves for the ground state energy of the many-body wave function by simulating the Schrödinger equation in imaginary

time, where V is the potential energy operator and E is an energy offset adjusted during the simulation to achieve a stationary solution when $\Psi(\mathbf{R},t)$ is an eigenfunction. Recognizing that eq 1 is essentially a diffusion equation, DMC calculates the energy of the wave function by simulating the dynamic evolution of a population of electronic configurations until they reach a steady-state solution.

$$\frac{\partial}{\partial t}\Psi(\mathbf{R},\,t) = \left(-\frac{1}{2}\nabla^2 + V - E\right)\Psi(\mathbf{R},\,t) \tag{1}$$

Because the wave function can take on both positive and negative values, ideally the electronic configurations should be assigned both positive and negative weights. However, doing so can make diffusion Monte Carlo calculations very inefficient.[28] To address this problem, a common approximation is to use a trial function, $\Psi_T(\mathbf{R},t)$, and enforce the constraint that the nodes of $\Psi(\mathbf{R},t)$ must match those of $\Psi_T(\mathbf{R},t)$ (i.e., $\Psi(\mathbf{R},t)$ must be zero when $\Psi_T(\mathbf{R},t)$ is zero). This is known as the "fixed-node" approximation.[29] If the nodal surface of the trial function is the same as that of the eigenfunction, DMC converges to the exact ground state energy, and for an approximate trial nodal surface, it produces a tight upper bound.

2.2. Test Set. To evaluate the accuracy of DMC for calculating the formation energies of materials, it is necessary to have a set of materials for which highly accurate 0 K experimental data exist. The Committee on Data for Science and Technology (CODATA)[30] has generated accurate thermodynamic data for 151 different substances, including 51 crystalline materials whose constituents are selected from different blocks of the periodic table which have likewise properties, following the "Standard Order of Arrangement" procedure. From these data it is possible to calculate experimental 0 K enthalpies of formation for 26 different materials. For the present study, we have eliminated one water-containing compound, $CdSO_4 \cdot 8/3H_2O$, due to the difficulty in experimentally determining the structure of water inside the material. We have also eliminated three uranium-containing materials and one thorium-containing material due to the challenges in running DFT calculations for such heavy elements. The enthalpies of formation for the remaining 21 materials were used to benchmark the automated DMC calculations. To calculate these enthalpies of formation, it was necessary to use DMC to calculate the energies of 39 materials and molecules.

2.3. High-Throughput Framework for DMC. There are a number of choices that must be made when running a diffusion Monte Carlo (DMC) calculation. For example, it is necessary to determine how to treat core electrons, generate and represent a trial wave function, discretize the simulation steps, and determine when the calculation has converged. In addition, crystalline materials pose the challenge of determining how to best use simulations in finite-sized unit cells to calculate the properties of a system that is effectively infinitely large. For each of these factors there is the usual trade-off between speed and accuracy, and the optimal choices are often made on a per-calculation basis. However, while running high-throughput approach calculations, it is necessary to automate the process of making such choices. In this section we describe the automated procedure we developed for the calculations described in this paper. Quantum Monte Carlo calculations were performed using the CASINO software package,[31] and density functional theory calculations were performed using Quantum ESPRES-
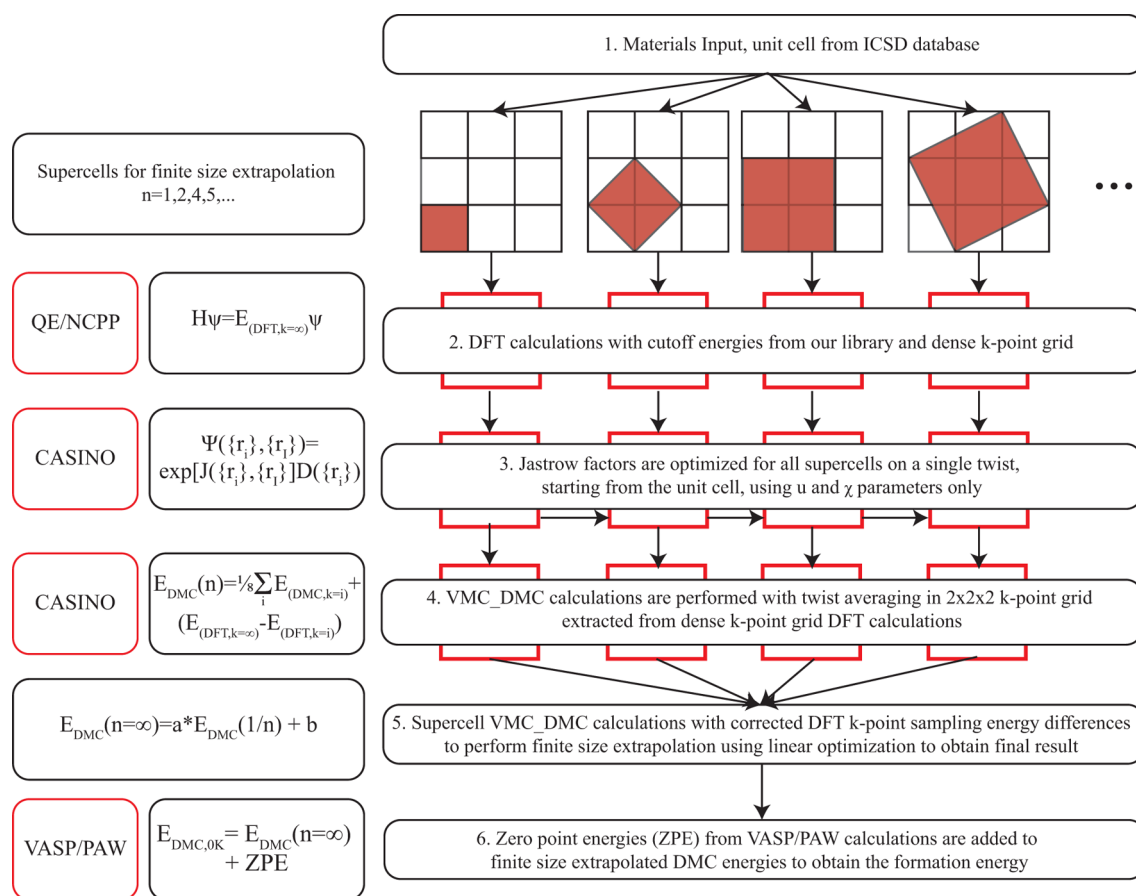
Figure 1. Automated DMC calculation scheme. Supercell sizes are only shown as representative. For the equations on the left side of the figure, n corresponds to an arbitrary size of the supercell used for finite size extrapolation, whereas k corresponds to the collection of grid points used for that calculation. In this respect, $k = i$ stands for one of the eight reciprocal cell grid points used in the DMC integration, and $E_{(DMC,k=i)}$ is the DMC energy of a structure integrated at single k-point i. The same notation has also been used for DFT calculations. QE[32]/NCPP, CASINO,[31] and VASP[33]/PAW[34] indicate the software used in the calculation and the pseudopotential used. NCPP and PAW stand for norm-conserving pseudopotential and projector augmented wave methods, respectively. $J[(r_i,r_j)]$ is the Slater-Jastrow factor where r_i and r_j represent electron and ion coordinates. $E_{DMC}(n = \infty)$ is the finite size extrapolated DMC energy, which is obtained by performing linear fitting to $E_{DMC}(n)$ values at the reciprocal of the supercell size, $1/n$. Finally, $E_{DMC,0\,K}$ corresponds to the formation energy of the structure at 0 K.

SO (QE) with norm-conserving pseudopotentials (NCPP).[32] In Figure 1, we show a schematic of the automated framework for DMC calculations. Compared to performing high-throughput DFT calculations, DMC calculations require additional steps that mainly arise from the errors in finite size extrapolation and k-point sampling in many-body interacting systems.

It is necessary to account for finite-size effects when running QMC calculations on periodic systems. Simulations are run in a single unit cell, which can introduce two sources of error. The first source of error is the approximation of continuous integrals over the Brillouin zone by sampling a discrete set of k-points. This error can be addressed by increasing the density of sampled k-points. Unlike DFT calculations, the cost of a DMC calculation scales better than linearly with the number of sampled k-points, because the statistical error in a DMC calculation scales with the total number of samples collected during the statistics accumulation phase, whether these samples are taken at a single k-point or spread among several k-points. The additional cost to sampling different k-points is therefore primarily due to the cost of running separate DMC equilibration steps for each k-point. The cost of sampling at different k-points can be further reduced by sampling only at k-points that are either multiples or half-multiples of reciprocal lattice vectors. These k-points represent periodic and antiperiodic wave functions, respectively, and the resulting DMC calculation can be executed using only real arithmetic, which can speed up the calculation by a factor of 4.[35]

We used a $2 \times 2 \times 2$ k-point grid for our calculations to maximize the sampling of the Brillouin zone without using complex arithmetic. However, in order to eliminate any potential undersampling of the Brillouin zone, we used the method similar to that proposed by Rajagopal et al.[36] Each DMC energy is calculated using a $2 \times 2 \times 2$ k-point grid corrected by the difference between a well-converged DFT energy and the DFT energy calculated using a $2 \times 2 \times 2$ grid. The well-converged DFT energies were calculated using a k-point grid with density of at least 8000 k-points per Å^{-3}. However, a $2 \times 2 \times 2$ k-point grid is generally not sufficient to ensure reliable convergence of the electronic self-consistency loop in DFT; therefore, the DFT energy for the $2 \times 2 \times 2$ grid was calculated by extracting the $2 \times 2 \times 2$ subset of k-points which is used to perform twist averaging[37] in the DMC calculations.

An additional finite-size error is introduced by the fact that QMC calculations are run in finite simulation cells that are

subject to periodic boundary conditions, so each electron interacts with its periodic images. To correct for this error, we calculated the energy per formula unit in supercells of three different sizes and extrapolated the results (after correcting for k-point sampling) to infinite system size using the extrapolation formula proposed by Ceperley and Alder[38] (eq 10 in their paper). All supercells were chosen to ensure the total number of electrons in the simulation cell was an even number. For a given supercell size N, several possible supercell shapes are possible. We selected the shape that maximized the minimum distance between periodic images. The supercells used for extrapolation were selected by starting with the minimum possible supercell size and then incrementing N until a supercell with a larger minimum distance between periodic images was found.

For each supercell, DFT was used to calculate the single-particle orbitals (Figure 1). The DFT calculations were performed in the generalized gradient approximation (GGA) with the Perdew−Burke−Ernzerhof (PBE) exchange-correlation functional using Quantum Espresso.[32] Gaussian smearing with a width of 0.02 Ry was used for Brillouin zone integration. All DFT calculations were run spin-polarized. To break symmetry, the initial magnetic moment was set to 0.7 for one randomly selected element in each material. The number of spin-up and spin-down electrons to be included in the QMC calculations was determined by sorting the DFT eigenvalues from lowest to highest and selecting the first N_{elect} orbitals, where N_{elect} is the total number of valence electrons in the simulation. For simulations in supercells, the net spin (# of up electrons − # of down electrons) was always rounded to a multiple of the number of primitive cells in the supercell. This resulted in a consistent net spin per unit cell across all supercell sizes. Of the compounds included in our test set, only molecular oxygen and $CuSO_4$ were found to have nonzero net spin. DFT calculations were performed using the same norm-conserving pseudopotentials (NCPP) used for DMC. Detailed information regarding pseudopotential selection can be found in Section 2.4. The orbitals calculated using DFT were used to generate the trial wave functions for VMC. The trial wave function, $\Psi_T(\mathbf{R},t)$, is expressed in Slater-Jastrow form using a single determinant

$$\Psi(\mathbf{R}, t) = D(\mathbf{R})e^{J(\mathbf{R})} \tag{2}$$

where $\mathbf{R}$ represents the positions of the electrons, $D(\mathbf{R})$ is a Slater determinant of the single-particle DFT orbitals, and $J(\mathbf{R})$, the Jastrow factor, is a parametrized function that approximately accounts for the effects of electron correlation. It has been found that compared to using a single determinant from Hartree−Fock calculations, DFT orbitals yield a better representation of the nodal surface, therefore leading to more accurate total and dissociation energies in atoms and diatomic molecules.[39] Using an accurate trial wave function in diffusion Monte Carlo reduces the localization error[21] and improves the efficiency of diffusion Monte Carlo. In this work, the following form was used

$$J(\mathbf{r}_i, \mathbf{r}_j) = \sum_{i=1}^{N-1}\sum_{j=i+1}^{N} u(\mathbf{r}_{ij}) + \sum_{i=1}^{N}\sum_{I=1}^{N_{ions}} \chi(\mathbf{r}_{iI}) + \sum_{i=1}^{N-1}\sum_{j=i+1}^{N} p(\mathbf{r}_{ij}) \tag{3}$$

where N is the number of electrons, N_{ions} is the number of ions, $\mathbf{r}_{ij} = \mathbf{r}_i - \mathbf{r}_j$, $\mathbf{r}_{iI} = \mathbf{r}_i - \mathbf{r}_I$, $\mathbf{r}_i$ is the position of electron i, and $\mathbf{r}_I$ is the position of ion I. $J(\mathbf{r}_i, \mathbf{r}_j)$ is the sum of isotropic electron−

electron terms, u, electron−nucleus term, χ, and plane-wave expansions of electron−electron separation, p. It was found that including three-body terms made relatively small improvements in the final results and made the optimization of Jastrow parameters less reliable.

The parameters in the Jastrow factor were optimized using VMC calculations with standard routines available in CASINO. In each of these calculations, the electronic configurations were propagated for 10,000 equilibration steps, and then an additional 150,000 steps were run to generate a sample of 10,000 random configurations. The VMC time step is internally optimized at every step during equilibration, aiming for 50% acceptance ratio in the Metropolis algorithm. The samples were taken every 15 steps to reduce serial correlation between samples. The parameters of the Jastrow factor were optimized to minimize the mean absolute deviation of the local energy E_L, defined as

$$E_L(R) = \frac{H\Psi(R)}{\Psi(R)} \tag{4}$$

For an eigenstate, the local energy will be constant for all electronic configurations, and the mean absolute deviation of the local energy will be zero.[29]

For large supercell sizes, we found that occasionally the optimization of the Jastrow factor would converge poorly (e.g., resulting in an anomalously high mean absolute deviation of the local energy), while for the smallest supercell sizes for each material the Jastrow factor converged reliably in all cases. Reliable convergence of the Jastrow factor at larger supercell sizes was achieved by initializing the Jastrow parameters for each supercell with the converged Jastrow parameters for the next-smallest supercell. It was found that the same Jastrow parameters worked nearly equally well at all k-points, so in our automated formulation the Jastrow parameters were optimized at a single k-point and used for the remaining seven k-points on the $2 \times 2 \times 2$ k-point grid.

The VMC-optimized Jastrow factors were used to generate trial wave functions for the DMC calculations. For the DMC simulations, a constant time step of 0.01 au was used. Casula's T-moves were used to improve the reliability of DMC calculations, as they make DMC energies variational, although this choice likely slightly increased the time-step error.[40] Using routines available in CASINO, checkpoints were created for the DMC calculations every 500 steps, and the calculation was restarted from the checkpoint if the weight exceeded the target weight by a factor of more than 8. The total number of samples collected for statistics was at least 80,000 times the number of valence electrons in the simulation. This number varied for different materials, as we explored different approaches and ensured we had enough samples to reach an acceptable level of accuracy in the calculated energies. The DMC-calculated energies were then extrapolated to infinite system size using the finite size extrapolation formula as proposed by Ceperley and Alder,[38] as discussed above.

For accurate comparisons with experiment, it necessary to include the zero-point vibrational energies. Zero-point vibrational energies for all structures were calculated using density functional theory as implemented in the Vienna Ab-initio Simulation Package (VASP) and settings used by the Materials Project.[6] The dynamical matrix was calculated using density functional perturbation theory for a supercell in which all possible lattice vectors were at least 8 Å. The zero-point energy
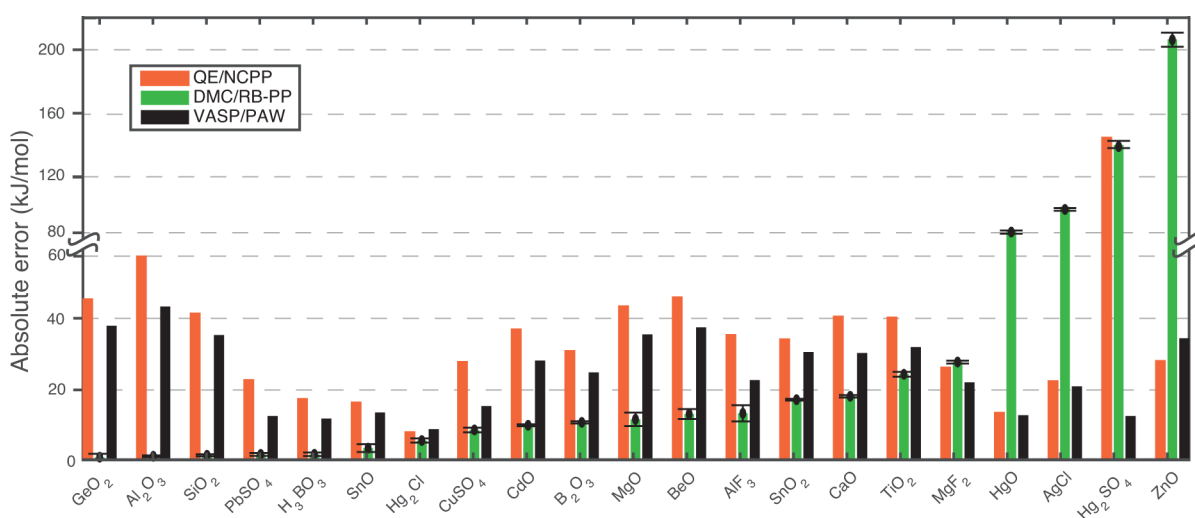
Figure 2. Absolute error per atom with respect to experimental formation energies for the compounds in the benchmark set using RB-PP. The QE/NCPP results are shown with orange, and DMC results are shown with blue bar histograms. Black error bar lines on DMC/RB-PP results represent the statistical error that results from the Monte Carlo algorithm. VASP/PAW results are shown with the black bar histograms. On the y-axis a break is placed between 60 and 80 kJ/mol and the upper half of the y-axis has larger intervals for better representation.

was calculated using PHONOPY.[41] To evaluate the accuracy of the calculated energies, the DFT-calculated zero-point energies were added to the DMC-calculated energies, and the sum was compared to the experimental formation enthalpies at 0 K. We neglected the pressure–volume contribution to the experimental formation enthalpy per atom, as this is negligible at a pressure of 1 atm.

2.4. Choice of Pseudopotentials. All QMC calculations were performed using norm-conserving or energy consistent pseudopotentials. Although previous work has shown improved DMC energies using Hartree–Fock pseudopotentials,[42] in our initial set of calculations we used DFT pseudopotentials because we found that the DFT/GGA self-consistency loop more reliably converged when using pseudopotentials generated for use with DFT/GGA calculations. We identify several works that perform total energy calculations on ZnO,[43−45] polymorphs of TiO$_2$,[46−48] different magnetic states of Ti$_4$O$_7$,[49] and superconductivity of several cuprates.[50,51] In these previous calculations, comparisons were made of the relative energies of different polymorphs, defect structures, or different magnetic configurations; however calculations for the Ti, Zn, or Cu metals were not included, preventing us from comparing formation energies to our present work.

For most elements the norm conserving Rappe-Bennett pseudopotentials (RB-PP)[52] generated by OPIUM[53] were used, but for some we found that the Fritz-Haber Institute pseudopotentials optimized in PBE (FHI-PP) generated by Scheffler et al.[54] gave more accurate results. For select cases with very poor accuracy, we tested Burkatzki-Filippi-Dolg (BFD-PP)[55] pseudopotentials and Optimized Troullier Martins (OPT-PP)[43] pseudopotentials, in order to provide additional comparisons. BFD-PP pseudopotentials are the only Gaussian basis pseudopotentials that we used among the pseudopotential sets that we investigated. In BFD-PP calculations, DFT calculations were performed using a triple-ζ Gaussian basis, with CRYSTAL code.[56] In all other DFT calculations, a plane-wave basis was used with Quantum Espresso code.[32] The cutoff energy for the plane-wave basis was determined by running a series of calculations on each of the pure elements, in which the cutoff energy was increased in increments of 10 Ry. The energy

was considered to have converged with respect to basis size when the calculated energy per atom changed by less than 1 meV/atom between successive increments. For materials or molecules containing multiple elements, the largest plane-wave cutoff energy among the elements was used. The pseudopotentials and cutoff energies used for each of the elements in this study are listed in the Supporting Information (SI).

3. RESULTS

In Figure 2, we show the results of our DMC calculations using the RB-PP for all compounds. We use these results as our reference and first attempt to utilize our DMC recipe. Up to Hg$_2$Cl$_2$ on the x-axis, DMC calculations are able to provide chemical accuracy, meaning that the results are within 1 kcal/mol per atom (4.12 kJ/mol per atom) of the experimental formation energies. These results are substantially more accurate than the corresponding DFT with errors ranging from 5 to 60 kJ/mol per atom for these materials. Continuing through to MgF$_2$, in Figure 2, DMC calculations showed improved accuracy compared to QE/NCPP calculations. However, for HgO, AgCl, Hg$_2$SO$_4$, and ZnO, DMC formation energy errors are larger than their QE/NCPP counterparts and in some cases by a considerable amount.

In order to understand these cases with large DMC errors we investigated several possible causes.[57] First was the use of asymmetric Casula T-move branching factors, which make the DMC energy variational and prevent population explosion errors when nonlocal pseudopotentials are used. The T-move scheme may also increase the localization error due to the pseudopotentials and yield a slightly larger time-step bias. An alternative is to use symmetric T-move branching factors, which have been shown to decrease the time-step bias further to some extent.[40] To evaluate whether large errors originate from time step extrapolation or our choice of T-move scheme, we compare the performance of the two Casula T-move schemes for SiO$_2$ and ZnO structures and perform time-step extrapolation to zero for total energies and formation energies of each compound (for additional details, see the SI). We show that the large error in the formation energy is not a result of the difference in Casula T-move implementation or choice of the
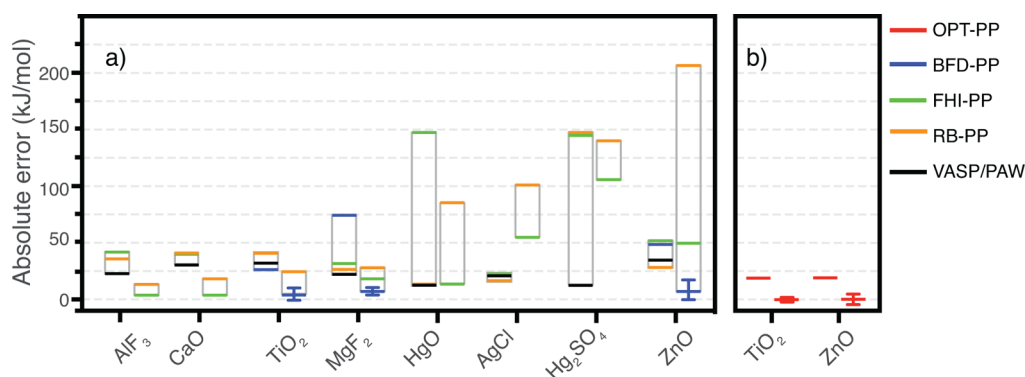
Figure 3. Absolute error per atom for the compounds which are identified to be problematic when RB-PP is used. Parts a) and b) use the same scale on the *y*-axis. However, they are separated as all the calculations in a) use the PBE method in DFT and orbital generation for QMC, whereas calculations in b) use LDA. Within each figure there are two groups of data for each compound, enclosed with a box if results of more than one pseudopotentials are compared. The first group, on the left, represents the DFT calculations, whereas the second group represents DMC calculations. Each color given in the legend shows the pseudopotential used in performing respective calculations. Error bars in DMC calculations are smaller than the thickness of the associated lines, if not shown explicitly. Tabulated values can be found in the SI.

time step, as the difference in formation energies at different time steps is within the error bar of the DMC results at 0.01 au.

Second, we investigate the pseudopotential errors in the Hamiltonian, as they are found to be rather large and nonsystematic especially for heavy elements.[24] Pseudopotentials can also affect the nodal surface and shape of the trial wave function, making it challenging to characterize and isolate the source of error being either the pseudopotential itself or the nodal surface of the trial wave function. Therefore, we perform benchmark calculations on select compounds using several pseudopotentials to understand if these errors can be controllable.

Among the test set materials considered in this work, compounds that include Zn, Hg, Ag, F, and Ti atoms tend to have the largest discrepancy between DMC and experimental results (Figure 2). To test the BFD-PP and OPT-PP pseudopotentials, we needed to make slight changes to our recipe. DFT calculations using BFD-PP were performed using the CRYSTAL code[56] at the PBE level using a double-ζ Gaussian basis. As OPT-PP are available for only first row transition metals and they are optimized for the local density approximation (LDA),[58] whenever there is a p-block element in a compound to be simulated, we combine it with Fritz-Haber Institute pseudopotentials optimized at the LDA level and perform DFT calculations to prepare trial wave functions using LDA. Therefore, only TiO_2 and ZnO in our test set could be simulated using OPT-PP.

We initially calculated the formation energies using RB-PP as shown in Figure 2. Then in Figure 3, for the problematic cases of Figure 2, we show that using FHI-PP leads to improved DMC formation enthalpies for most compounds compared to using RB-PP. For example, AlF_3 and CaO have errors of less than 5 kJ/mol per atom in the DMC/FHI-PP calculations, compared to 13.3 ± 2.3 and 18.1 ± 0.3 kJ/mol atoms for the DMC/RB-PP results. For transition metal containing compounds and MgF_2 however, still DMC/FHI-PP results are not significantly better than VASP/PAW calculations. For TiO_2, both DMC/OPT-PP and DMC/BFD-PP perform substantially better compared to DMC/RB-PP and VASP/PAW. For MgF_2, we could only perform DMC/FHI, DMC/BFD, and DMC/RB calculations, since the pseudopotential for Mg does not exist in the OPT-PP set. For ZnO however, DMC calculations substantially improve when OPT-PP and BFD-PP are used,

resulting in errors of less than 7.1 kJ/mpmol atom. With this understanding of the performance of the pseudopotentials, in Figure 4, we show the combined benchmark results from Figures 2 and 3. In Figure 4, except for all compounds containing F, Ca, Ti, Hg and Zn, we used RB-PP (see SI for details). Eliminating finite size errors in metallic materials can be especially challenging due to the complex shape of the Fermi surface, which may require denser *k*-point sampling. However, the accurate results obtained for these compounds, using BFD and OPT-PP, show that for the cases considered here pseudopotentials are the largest source of error, and our recipe yields transferable performance given the use of suitable pseudopotentials.

4. DISCUSSION

We show that an automated, simple recipe to perform QMC calculations can be used to provide increased accuracy icompared to DFT, in formation energies of periodic solids. For a test set of 21 compounds (see Figure 4) with experimentally known formation energies, chemical accuracy was obtained with our automated DMC recipe for 11 structures. DFT calculations using either the QE/NCPP or VASP/DFT methods were not able to provide chemical accuracy in any of the compounds. Overall, for 18 of the 21 compounds, our DMC recipe provides results with significantly improved accuracy compared to VASP/PAW. We find that for the three remaining cases, AgCl, HgO, and Hg_2SO_4, DMC performs worse than VASP/PAW. Among these, the DMC errors are anomalously high for two of the compounds: AgCl and Hg_2SO_4. Because there are currently no BFD or OPT pseudopotentials available for Ag or Hg, we were only able to generate results for these compounds using the RB and FHI pseudopotentials. Based on our tests on ZnO, TiO_2, and MgF_2, we believe the RB and FHI pseudopotentials for Ag and Hg are likely the source of the anomalously high error.

We note that the high-throughput DFT recipes make use of empirical fitting schemes for elemental energies, whereas our QMC calculations use no empirical fitting parameters. Saal et al.[1] compared the performance of high-throughput DFT recipes over two of the existing databases: Materials Project[6,57] and Open Quantum Materials Database (OQMD).[1] Formation energies of 1386 compounds found in Materials Project are compared with respect to experimental energies when two
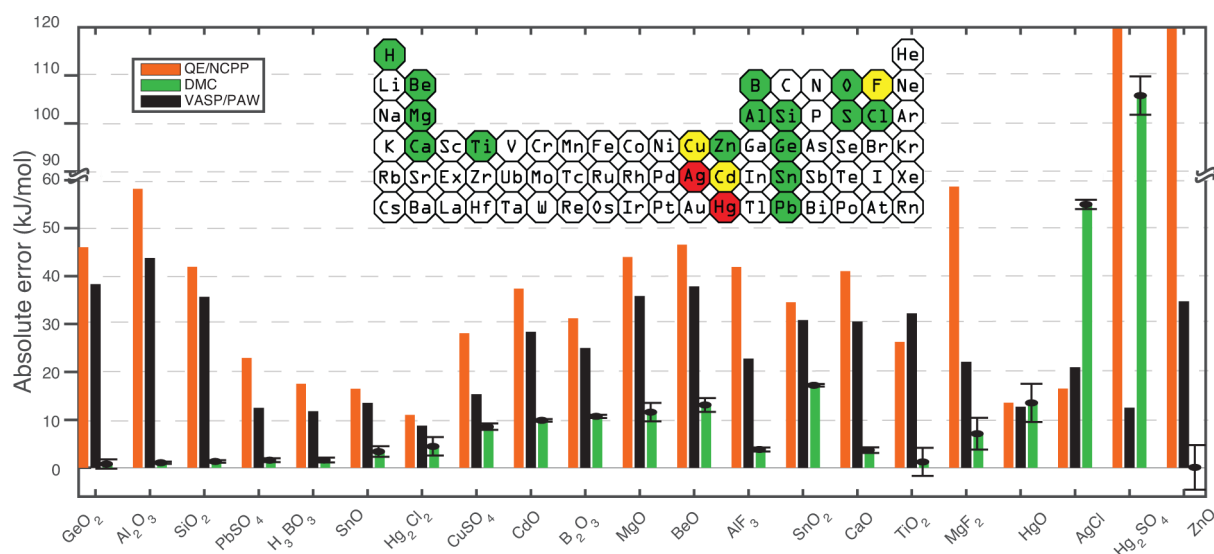
Figure 4. Absolute error per atom for the benchmark set using RB-PP for all atoms except for the compounds containing F, Ca, Ti, Hg, Ag, and Zn. For the compounds which contain these atoms, results here are taken from the best DMC calculation in Figure 3. Bar histograms are represented in the same way as Figure 2. The periodic table in the inset represents the atoms that perform with desirable accuracy in green, with slightly worse accuracy in yellow, and atoms whose pseudopotentials need improvement in red. On the y-axis a break is placed between 60 and 90 kJ/mol for better representation. Similarly, QE/NCPP values for Hg_2SO_4 and ZnO are not shown as the graph is truncated at 120 kJ/mol. These values are 147.41 and 237 kJ/mol, respectively. Tabulated values can be found in the SI.

recipes are employed yielding 0.133 eV/atom and 0.108 eV/atom mean absolute errors (MAE). Within the OQMD recipe, when only binary compounds are investigated, the resulting MAE is 0.119 eV/atom. In comparison, our QMC recipe yields a MAE of 0.058(6) eV/atom (when compounds that rely on Ag and Hg pseudopotentials are excluded, such as AgCl, Hg_2SO_4, HgO, Hg_2Cl_2, MAE is 0.028(5) eV/atom), whereas pure DFT-GGA calculations we performed with VASP/PAW yield a MAE of 0.276 ev/atom over the same set.

Although our results show that performing DMC calculations in a preset scheme on a range of materials can provide significantly improved accuracy over DFT calculations, pseudopotential errors are nonsystematic in DMC and can, for a small number of cases, lead to serious errors. Given that an improvement over DFT was obtained in 85% of the cases tested here, the simple, automated approach we present may be sufficient for a host of applications. We find that pseudopotentials that perform accurately in DFT do not necessarily perform as well in QMC. In Table 1, we show the differences between the tested pseudopotentials for the two transition metals we investigated in detail, Zn and Ti. Both BFD-PP and

OPT-PP use a Ne core for first row transition metals as it was found that semicore effects can be crucial.[43] These PP also have relatively smaller core radii on the d orbitals. Additionally, BFD-PP uses an energy consistent scheme rather than norm-conserving, as they found that energy consistent pseudopotentials can give more accurate results in MP2, CCSD(T), and DMC calculations.[55] On the other hand, OPT-PP uses very small nonlocal radii, <1 au, to increase its transferability. It has been suggested that inclusion of higher angular momentum channels and using them as the local channel for a pseudopotential can lead to improved energies in QMC calculations.[59] However, in our comparisons between different pseudopotentials, we see the smaller core radius and larger number of valence electrons as an important indicator for accuracy.

■ ASSOCIATED CONTENT

Ⓢ Supporting Information

The Supporting Information is available free of charge on the ACS Publications website at DOI: 10.1021/acs.jctc.6b01179.

> Pseudopotentials used in the study and in Figure 4, ICSD sample numbers for the unit cells of calculated crystals, explicit values in Figures 2, 3, and 4, and time step extrapolation tests with two implementations of the Casula T-move scheme and finite size extrapolations for BFD-PP and OPT-PP (ZIP)

■ AUTHOR INFORMATION

Corresponding Author
*E-mail: jcg@mit.edu.

ORCID Ⓞ
Kayahan Saritas: 0000-0002-2240-8520

Notes
The authors declare no competing financial interest.

Table 1. Comparison between All Investigated Pseudopotentials for Zn and Ti for Valence Electrons, d-Orbital Core Radii, Local and Highest Angular Momentum (l) Channels

	OPT-PP	BFD-PP	FHI-PP	RB-PP
Number of Valence Electrons (Z_{eff})				
Zn	20	20	12	12
Ti	12	12	4	12
d-Orbital Core Radii (in au)				
Zn	0.80	1.16	2.37	1.97
Ti	0.80	1.60	2.71	1.70
Local and Highest l Channels				
Zn	p,d	d,d	s,d	s,d
Ti	p,d	d,d	p,d	s,d

◼ REFERENCES

(1) Saal, J. E.; Kirklin, S.; Aykol, M.; Meredig, B.; Wolverton, C. Materials Design and Discovery with High-Throughput Density Functional Theory: The Open Quantum Materials Database (OQMD). *JOM* **2013**, *65*, 1501−1509.

(2) Jain, A.; Ong, S. P.; Hautier, G.; Chen, W.; Richards, W. D.; Dacek, S.; Cholia, S.; Gunter, D.; Skinner, D.; Ceder, G.; Persson, K. a. The Materials Project: A Materials Genome Approach to Accelerating Materials Innovation. *APL Mater.* **2013**, *1*, 011002.

(3) Kohn, W.; Sham, L. J. Self-Consistent Equations Including Exchange and Correlation Effects. *Phys. Rev.* **1965**, *140*, A1133−A1138.

(4) Hohenberg, P.; Kohn, W. Inhomogeneous Electron Gas. *Phys. Rev.* **1964**, *136*, B864−B871.

(5) Perdew, J. P.; Burke, K.; Ernzerhof, M. Generalized Gradient Approximation Made Simple. *Phys. Rev. Lett.* **1996**, *77*, 3865−3868.

(6) Jain, A.; Hautier, G.; Moore, C. J.; Ong, S. P.; Fischer, C. C.; Mueller, T.; Persson, K. A.; Ceder, G. A high-throughput infrastructure for density functional theory calculations. *Comput. Mater. Sci.* **2011**, *50*, 2295−2310.

(7) Zhou, F.; Cococcioni, M.; Marianetti, C. A.; Morgan, D.; Ceder, G. First-principles Prediction of Redox Potentials in Transition-metal Compounds with LDA+U. *Phys. Rev. B: Condens. Matter Mater. Phys.* **2004**, *70*, 235121.

(8) Wang, L.; Maxisch, T.; Ceder, G. Oxidation Energies of Transition Metal Oxides within the GGA+U Framework. *Phys. Rev. B: Condens. Matter Mater. Phys.* **2006**, *73*, 195107.

(9) Chase, M. W. J. *NIST-JANAF Thermochemical Tables*, 4th ed.; American Institute of Physics: New York, 1998.

(10) Perdew, J. P.; Ernzerhof, M.; Burke, K. Rationale for Mixing Exact Exchange with Density Functional Approximations. *J. Chem. Phys.* **1996**, *105*, 9982−9985.

(11) Hedin, L. New Method for Calculating the One-Particle Green's Function with Application to the Electron-Gas Problem. *Phys. Rev.* **1965**, *139*, A796−A823.

(12) Shulenburger, L.; Mattsson, T. R. Quantum Monte Carlo applied to solids. *Phys. Rev. B: Condens. Matter Mater. Phys.* **2013**, *88*, 245117.

(13) Narayan, A.; Bhutani, A.; Rubeck, S.; Eckstein, J. N.; Shoemaker, D. P.; Wagner, L. K. Computational and Experimental Investigation for New Transition Metal Selenides and Sulfides: The Importance of Experimental Verification for Stability. *Phys. Rev. B: Condens. Matter Mater. Phys.* **2016**, *94*, 045105.

(14) Nemec, N. Diffusion Monte Carlo: Exponential Scaling of Computational Cost for Large Systems. *Phys. Rev. B: Condens. Matter Mater. Phys.* **2010**, *81*, 035119.

(15) Foulkes, W. M. C.; Mitas, L.; Needs, R. J.; Rajagopal, G. Quantum Monte Carlo simulations of solids. *Rev. Mod. Phys.* **2001**, *73*, 33−83.

(16) Williamson, A. J.; Hood, R. Q.; Grossman, J. C. Linear-Scaling Quantum Monte Carlo Calculations. *Phys. Rev. Lett.* **2001**, *87*, 246406.

(17) Reboredo, F. A.; Williamson, A. J. Optimized Nonorthogonal Localized Orbitals for Linear Scaling Quantum Monte Carlo Calculations. *Phys. Rev. B: Condens. Matter Mater. Phys.* **2005**, *71*, 121105.

(18) Needs, R. J.; Towler, M. D.; Drummond, N. D.; López Ríos, P. Continuum Cariational and Diffusion Quantum Monte Carlo Calculations. *J. Phys.: Condens. Matter* **2010**, *22*, 023201.

(19) Shao, Y.; Molnar, L. F.; Jung, Y.; Kussmann, J.; Ochsenfeld, C.; Brown, S. T.; Gilbert, A. T.; Slipchenko, L. V.; Levchenko, S. V.; O'Neill, D. P.; DiStasio, R. A., Jr; Lochan, R. C.; Wang, T.; Beran, G. J.; Besley, N. A.; Herbert, J. M.; Yeh Lin, C.; van Voorhis, T.; Hung Chien, S.; Sodt, A.; Steele, R. P.; Rassolov, V. A.; Maslen, P. E.; Korambath, P. P.; Adamson, R. D.; Austin, B.; Baker, J.; Byrd, E. F. C.; Dachsel, H.; Doerksen, R. J.; Dreuw, A.; Dunietz, B. D.; Dutoi, A. D.; Furlani, T. R.; Gwaltney, S. R.; Heyden, A.; Hirata, S.; Hsu, C.-P.; Kedziora, G.; Khalliulin, R. Z.; Klunzinger, P.; Lee, A. M.; Lee, M. S.; Liang, W.; Lotan, I.; Nair, N.; Peters, B.; Proynov, E. I; Pieniazek, P. A.; Min Rhee, Y.; Ritchie, J.; Rosta, E.; David Sherrill, C.; Simmonett, A. C.; Subotnik, J. E.; Lee Woodcock, H., III; Zhang, W.; Bell, A. T.; Chakraborty, A. K.; Chipman, D. M.; Keil, F. J.; Warshel, A.; Hehre, W. J.; Schaefer, H. F., III; Kong, J.; Krylov, A. I.; Gill, P. M. W.; Head-Gordon, M. Advances in Methods and Algorithms in a Modern Quantum Chemistry Program Package. *Phys. Chem. Chem. Phys.* **2006**, *8*, 3172−3191.

(20) Grossman, J. C. Benchmark quantum Monte Carlo calculations. *J. Chem. Phys.* **2002**, *117*, 1434−1440.

(21) Kolorenc, J.; Mitas, L. Applications of quantum Monte Carlo methods in condensed systems. *Rep. Prog. Phys.* **2011**, *74*, 026502.

(22) Krogel, J. T. Nexus: A Modular Workflow Management System for Quantum Simulation Codes. *Comput. Phys. Commun.* **2016**, *198*, 154−168.

(23) Santana, J. A.; Krogel, J. T.; Kent, P. R. C.; Reboredo, F. A. Cohesive energy and structural parameters of binary oxides of groups IIA and IIIB from diffusion quantum Monte Carlo. *J. Chem. Phys.* **2016**, *144*, 174707.

(24) Nazarov, R.; Shulenburger, L.; Morales, M.; Hood, R. Q. Benchmarking the Pseudopotential and Fixed Node Approximations in Diffusion Monte Carlo Calculations of Molecules and Solids. *Phys. Rev. B: Condens. Matter Mater. Phys.* **2016**, *93*, 094111.

(25) Wagner, L. K.; Ceperley, D. M. Discovering Correlated Fermions Using Quantum Monte Carlo. *Rep. Prog. Phys.* **2016**, *79*, 094501.

(26) Kolorenč, J. c. v.; Mitas, L. Quantum Monte Carlo Calculations of Structural Properties of FeO Under Pressure. *Phys. Rev. Lett.* **2008**, *101*, 185502.

(27) Austin, B. M.; Zubarev, D. Y.; Lester, W. A. Quantum Monte Carlo and related approaches. *Chem. Rev.* **2012**, *112*, 263−288.

(28) Berg, E.; Metlitski, M. A.; Sachdev, S. Sign-Problem−Free Quantum Monte Carlo of the Onset of Antiferromagnetism in Metals. *Science* **2012**, *338*, 1606−1609.

(29) Ceperley, D. M.; Alder, B. J. Ground State of the Electron Gas by a Stochastic Method. *Phys. Rev. Lett.* **1980**, *45*, 566−569.

(30) Franck, E. U. J. D. Cox, D. D. Wagman, V. A. Medvedev: CODATA Key Values for Thermodynamics, aus der Reihe: CODATA, Series on Thermodynamic Properties. Hemisphere Publishing Corporation, New York, Washington, Philadelphia, London 1989. 271 Seiten, Preis: £ 28.00. *Ber. der Bunsenges. Phys. Chem.* **1990**, *94*, 93−93.

(31) Towler, M. D. Casino Manual 2015. http://www.tcm.phy.cam.ac.uk/~mdt26/casino_manual_dir/casino_manual.pdf (accessed 2016-10-17).

(32) Giannozzi, P.; Baroni, S.; Bonini, N.; Calandra, M.; Car, R.; Cavazzoni, C.; Ceresoli, D.; Chiarotti, G. L.; Cococcioni, M.; Dabo, I.; Corso, A. D.; de Gironcoli, S.; Fabris, S.; Fratesi, G.; Gebauer, R.; Gerstmann, U.; Gougoussis, C.; Kokalj, A.; Lazzeri, M.; Martin-Samos, L.; Marzari, N.; Mauri, F.; Mazzarello, R.; Paolini, S.; Pasquarello, A.; Paulatto, L.; Sbraccia, C.; Scandolo, S.; Sclauzero, G.; Seitsonen, A. P.; Smogunov, A.; Umari, P.; Wentzcovitch, R. M. QUANTUM ESPRESSO: a Modular and Open-source Software Project for Quantum Simulations of Materials. *J. Phys.: Condens. Matter* **2009**, *21*, 395502.

(33) Kresse, G.; Hafner, J. Ab initio Molecular Dynamics for Liquid Metals. *Phys. Rev. B: Condens. Matter Mater. Phys.* **1993**, *47*, 558−561.

(34) Kresse, G.; Joubert, D. From Ultrasoft Pseudopotentials to the Projector Augmented-wave Method. *Phys. Rev. B: Condens. Matter Mater. Phys.* **1999**, *59*, 1758−1775.

(35) Drummond, N. D.; Needs, R. J.; Sorouri, A.; Foulkes, W. M. C. Finite-size Errors in Continuum Quantum Monte Carlo Calculations. *Phys. Rev. B: Condens. Matter Mater. Phys.* **2008**, *78*, 125106.

(36) Rajagopal, G.; Needs, R. J.; Kenny, S.; Foulkes, W. M. C.; James, A. Quantum Monte Carlo Calculations for Solids Using Special *k* Points Methods. *Phys. Rev. Lett.* **1994**, *73*, 1959−1962.

(37) Lin, C.; Zong, F. H.; Ceperley, D. M. Twist-averaged boundary conditions in continuum quantum monte carlo algorithms. *Phys. Rev. E: Stat. Phys., Plasmas, Fluids, Relat. Interdiscip. Top.* **2001**, *64* (1), 016702.

(38) Ceperley, D. M.; Alder, B. J. Ground State of Solid Hydrogen at High Pressures. *Phys. Rev. B: Condens. Matter Mater. Phys.* **1987**, *36*, 2092−2106.

(39) Per, M. C.; Walker, K. A.; Russo, S. P. How Important is Orbital Choice in Single-Determinant Diffusion Quantum Monte Carlo Calculations? *J. Chem. Theory Comput.* **2012**, *8*, 2255−2259.

(40) Casula, M.; Moroni, S.; Sorella, S.; Filippi, C. Size-consistent Variational Approaches to Nonlocal Pseudopotentials: Standard and Lattice Regularized Diffusion Monte Carlo Methods Revisited. *J. Chem. Phys.* **2010**, *132*, 154113.

(41) Togo, A.; Tanaka, I. First-principles Phonon Calculations in Materials Science. *Scr. Mater.* **2015**, *108*, 1−5.

(42) Greeff, C. W.; Lester, W. A. A soft Hartree-Fock pseudopotential for carbon with application to quantum Monte Carlo. *J. Chem. Phys.* **1998**, *109*, 1607−1612.

(43) Krogel, J. T.; Santana, J. A.; Reboredo, F. A. Pseudopotentials for Quantum Monte Carlo Studies of Transition Metal Oxides. *Phys. Rev. B: Condens. Matter Mater. Phys.* **2016**, *93*, 075143.

(44) Yu, J.; Wagner, L. K.; Ertekin, E. Towards a Systematic Assessment of Errors in Diffusion Monte Carlo Calculations of Semiconductors: Case Study of Zinc Selenide and Zinc Oxide. *J. Chem. Phys.* **2015**, *143*, 224707.

(45) Santana, J. A.; Krogel, J. T.; Kim, J.; Kent, P. R. C.; Reboredo, F. A. Structural Stability and Defect Energetics of ZnO from Diffusion Quantum Monte Carlo. *J. Chem. Phys.* **2015**, *142*, 164705.

(46) Abbasnejad, M.; Shojaee, E.; Mohammadizadeh, M. R.; Alaei, M.; Maezono, R. Quantum Monte Carlo Study of High Pressure Cubic TiO2. *Appl. Phys. Lett.* **2012**, *100*, 261902.

(47) Trail, J.; Monserrat, B.; López Ríos, P.; Maezono, R.; Needs, R. J. Quantum Monte Carlo Study of the Energetics of the Rutile, Anatase, Brookite, and Columbite TiO_2 Polymorphs. *Phys. Rev. B: Condens. Matter Mater. Phys.* **2017**, *95*, 121108.

(48) Luo, Y.; Benali, A.; Shulenburger, L.; Krogel, J. T.; Heinonen, O.; Kent, P. R. C. Phase Stability of TiO2 Polymorphs from Diffusion Quantum Monte Carlo. *New J. Phys.* **2016**, *18*, 113049.

(49) Benali, A.; Shulenburger, L.; Krogel, J. T.; Zhong, X.; Kent, P. R. C.; Heinonen, O. Quantum Monte Carlo Analysis of a Charge Ordered Insulating Antiferromagnet: the Ti4O7 Magneli Phase. *Phys. Chem. Chem. Phys.* **2016**, *18*, 18323−18335.

(50) Wagner, L. K.; Abbamonte, P. Effect of electron correlation on the electronic structure and spin-lattice coupling of high-T_c cuprates: Quantum Monte Carlo calculations. *Phys. Rev. B: Condens. Matter Mater. Phys.* **2014**, *90*, 125129.

(51) Foyevtsova, K.; Krogel, J. T.; Kim, J.; Kent, P. R. C.; Dagotto, E.; Reboredo, F. A. Ab initio Quantum Monte Carlo Calculations of Spin Superexchange in Cuprates: The Benchmarking Case of Ca2CuO3. *Phys. Rev. X* **2014**, *4*, 031003.

(52) Rappe-Bennett Pseudopotentials. http://www.sas.upenn.edu/rappegroup/research/pseudo-potential-gga.html (accessed 2016-10-11).

(53) OPIUM Pseudopotential Generator. http://opium.sourceforge.net (accessed 2016-10-11).

(54) Fuchs, M.; Scheffler, M. Ab Initio Pseudopotentials for Electronic Structure Calculations of Polyatomic Systems using Density Functional Theory. *Comput. Phys. Commun.* **1999**, *119*, 67−98.

(55) Burkatzki, M.; Filippi, C.; Dolg, M. Energy Consistent Pseudopotentials for Quantum Monte Carlo Calculations. *J. Chem. Phys.* **2007**, *126*, 234105.

(56) Dovesi, R.; Orlando, R.; Civalleri, B.; Roetti, C.; Saunders, V. R.; Zicovich-Wilson, C. M. CRYSTAL: a Computational Tool for the Ab-initio Study of the Electronic Properties of Crystals. *Z. Kristallogr. - Cryst. Mater.* **2005**, *220*, ssss DOI: 10.1524/zkri.220.5.571.65065.

(57) Jain, A.; Ong, S. P.; Hautier, G.; Chen, W.; Richards, W. D.; Dacek, S.; Cholia, S.; Gunter, D.; Skinner, D.; Ceder, G.; Persson, K. A. Commentary: The Materials Project: A Materials Genome Approach to Accelerating Materials Innovation. *APL Mater.* **2013**, *1*, 011002.

(58) Perdew, J. P.; Zunger, A. Self Interaction Correction to Density Functional Approximations for Many Electron Systems. *Phys. Rev. B: Condens. Matter Mater. Phys.* **1981**, *23*, 5048−5079.

(59) Tipton, W. W.; Drummond, N. D.; Hennig, R. G. Importance of High Angular Momentum Channels in Pseudopotentials for Quantum Monte Carlo. *Phys. Rev. B: Condens. Matter Mater. Phys.* **2014**, *90*, 125110.

I